Impact of paramagnetic Cu^{II} and diamagnetic Zn^{II} ions on single-molecule magnetism in heterodinuclear 3d–4f complexes displaying slow relaxation of magnetization

Rakhi Nandy[a] Narayan Ch. Jana,[b] Marko Jagodič,[c] Zvonko Jagličić,[c,d] Paula Brandão,[e] Amrita Saha,[f] and Anangamohan Panja[a,b]

[a]*Department of Chemistry, Gokhale Memorial Girls' College, 1/1 Harish Mukherjee Road, Kolkata 700020, India, E-mail: ampanja@yahoo.co.in*

[b]*Department of Chemistry, Panskura Banamali College, Panskura RS, WB 721152, India.*

[c]*Institute of Mathematics, Physics and Mechanics, Jadranska 19, 1000 Ljubljana, Slovenia*

[d]*University of Ljubljana, Faculty of Civil and Geodetic Engineering, Jamova cesta 2, 1000 Ljubljana, Slovenia*

[e]*Department of Chemistry, CICECO-Aveiro Institute of Materials, University of Aveiro, 3810-193 Aveiro, Portugal*

[f] *Department of Chemistry, Jadavpur University, Kolkata 700032, India*

Contents

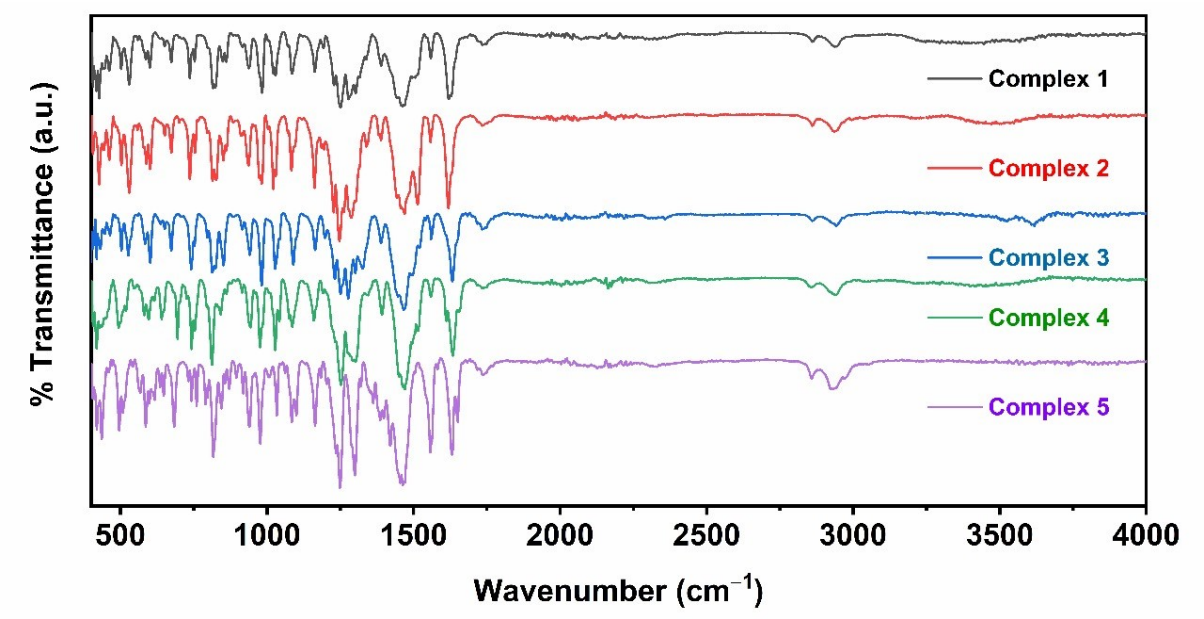

Fig. S1. IR spectra of complexes **1-5**.

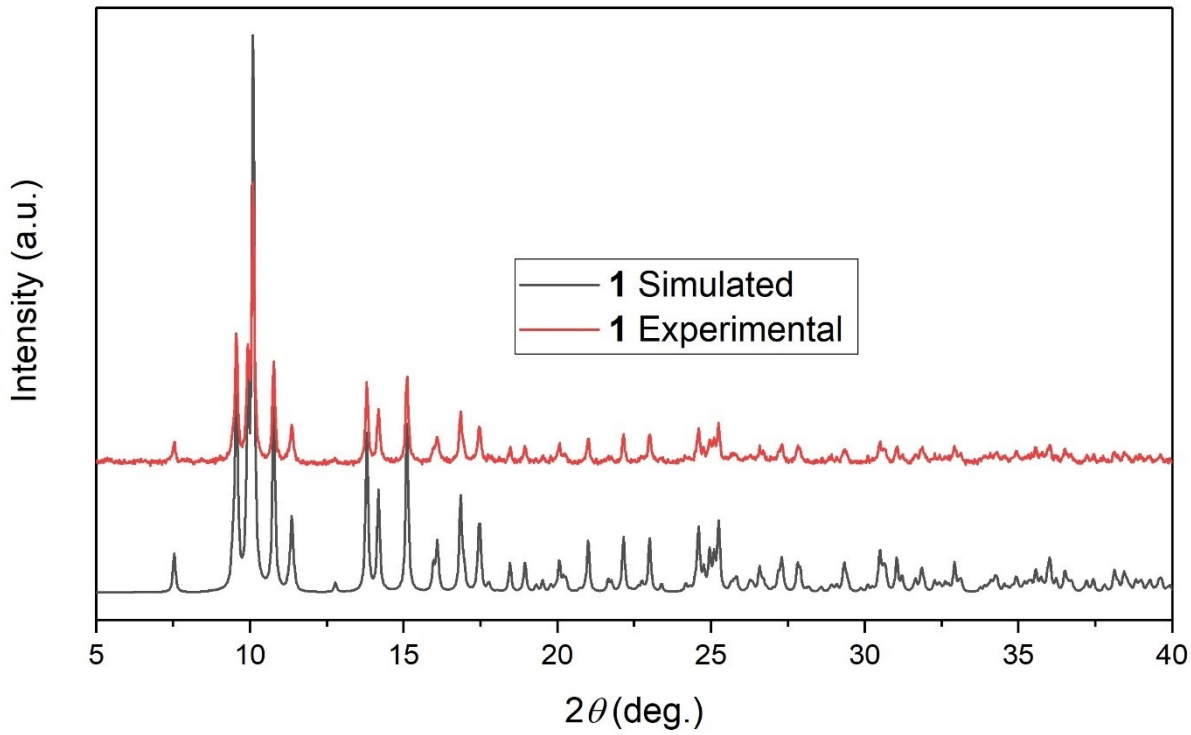

Fig. S2: PXRD spectra of the complexes **1**.

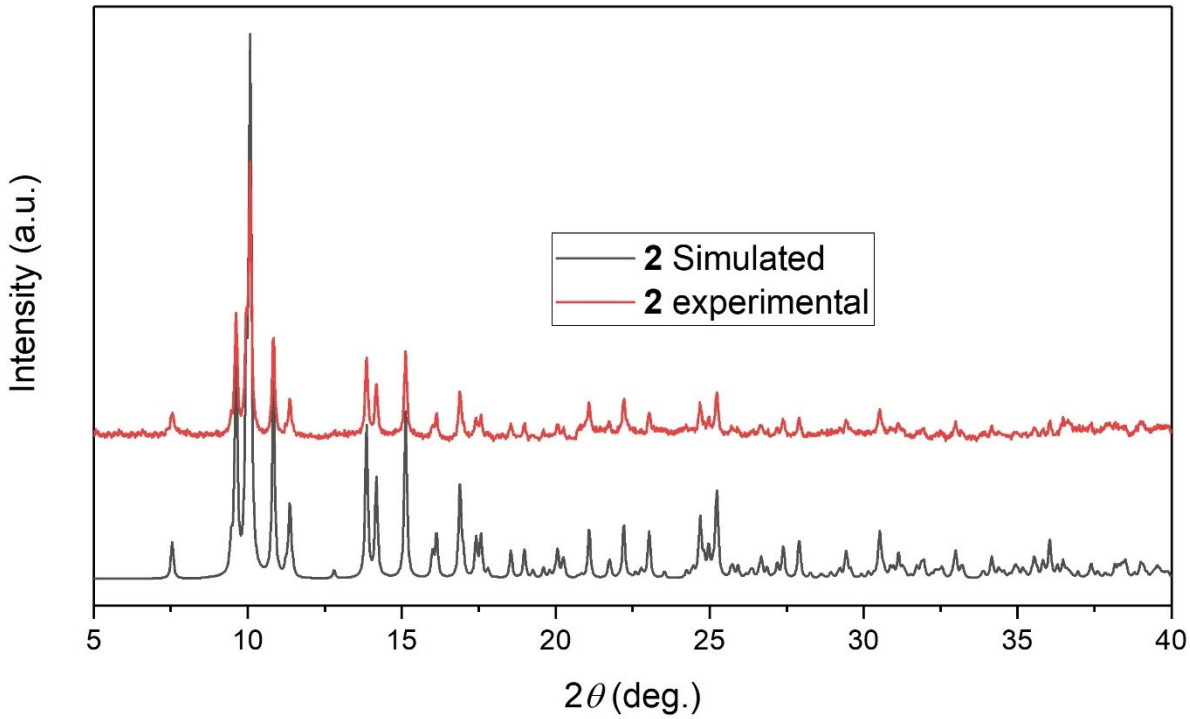

Fig. S3: PXRD spectra of the complexes **2**.

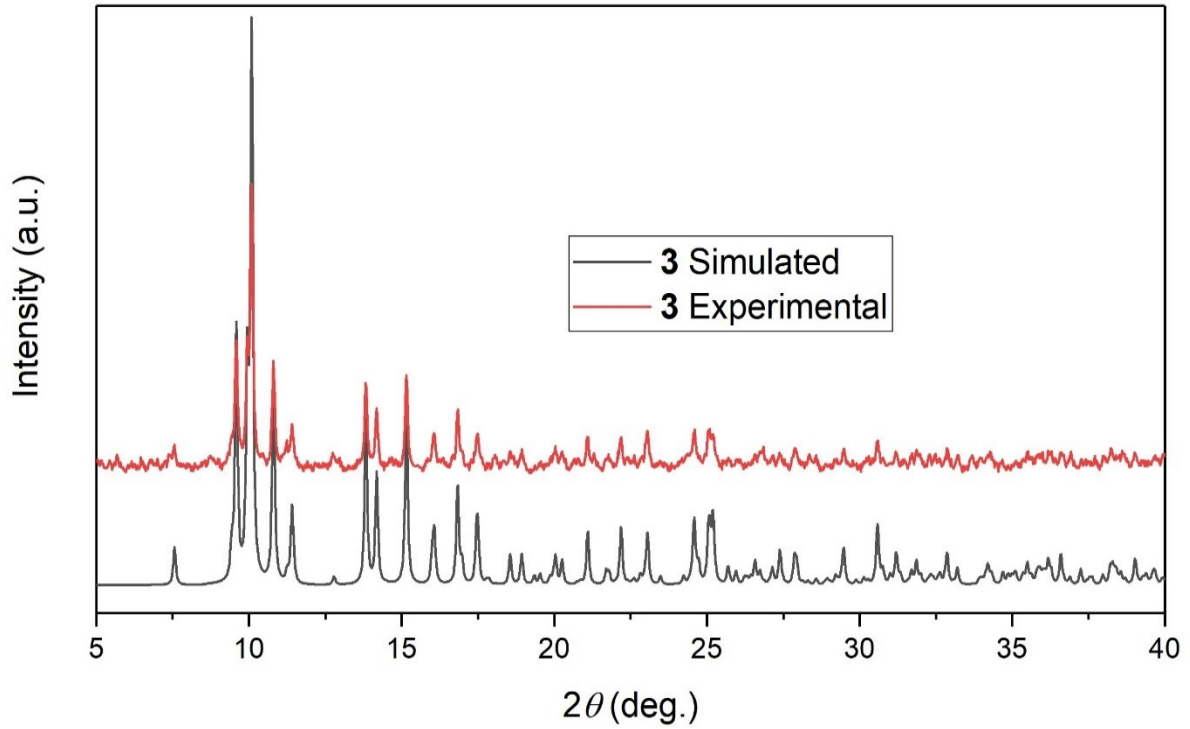

Fig. S4: PXRD spectra of the complexes 3.

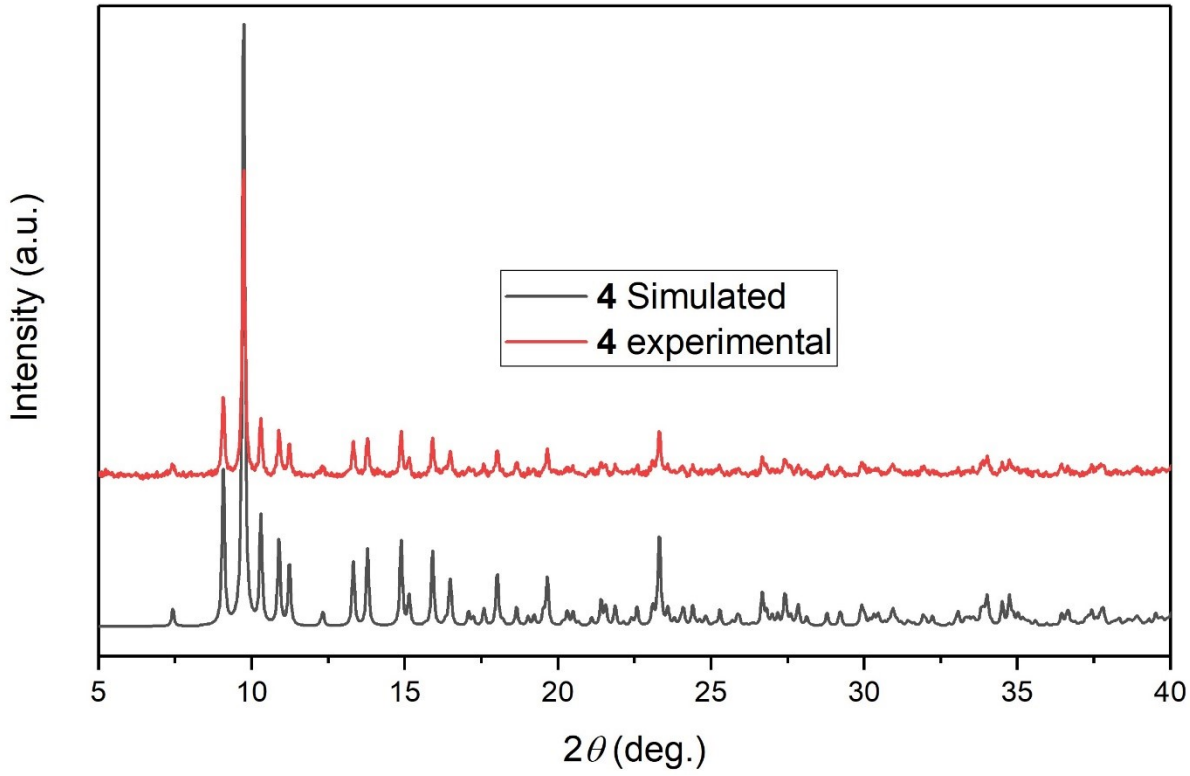

Fig. S5: PXRD spectra of the complexes **4**.

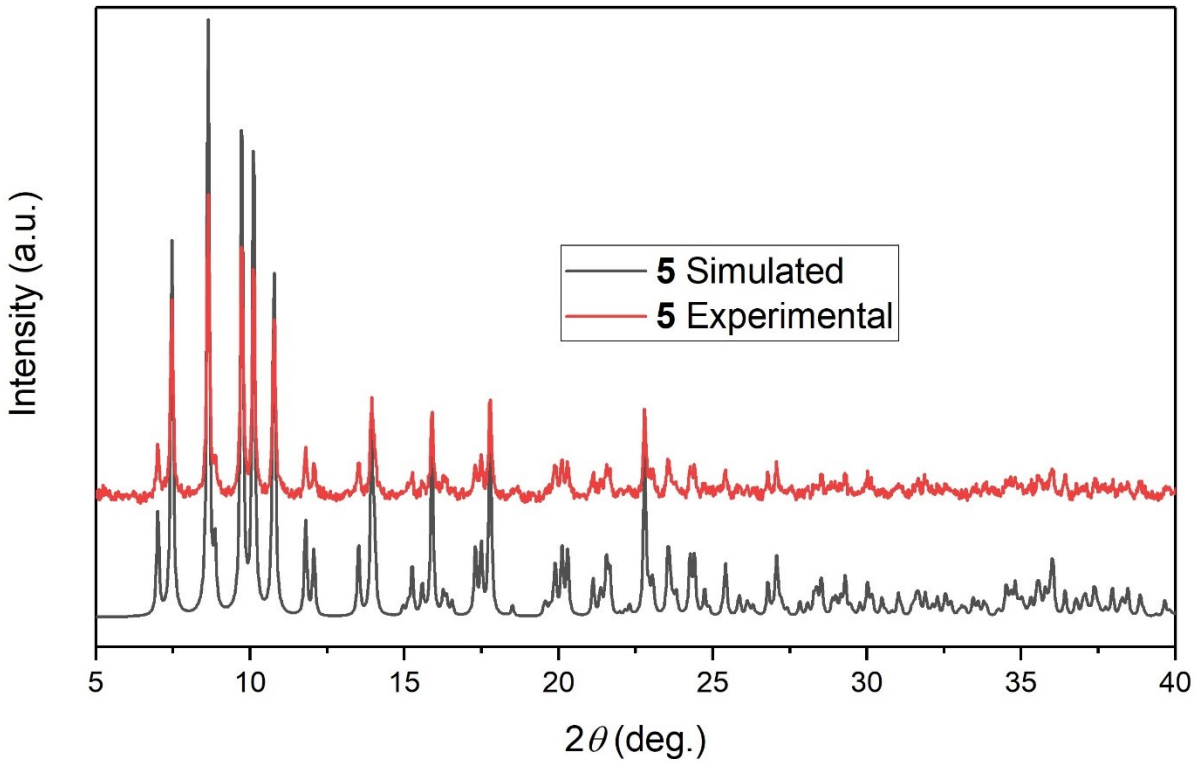

Fig. S6: PXRD spectra of the complexes 5.

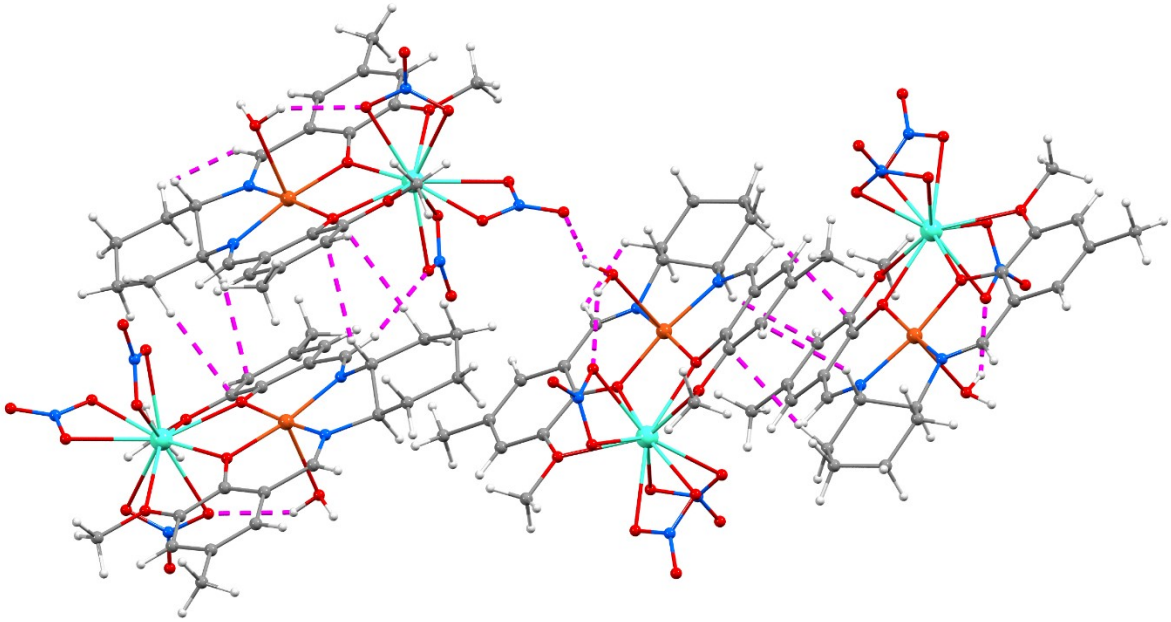

Fig. S7. A part of molecular packing showing different non-covalent interactions in **1**.

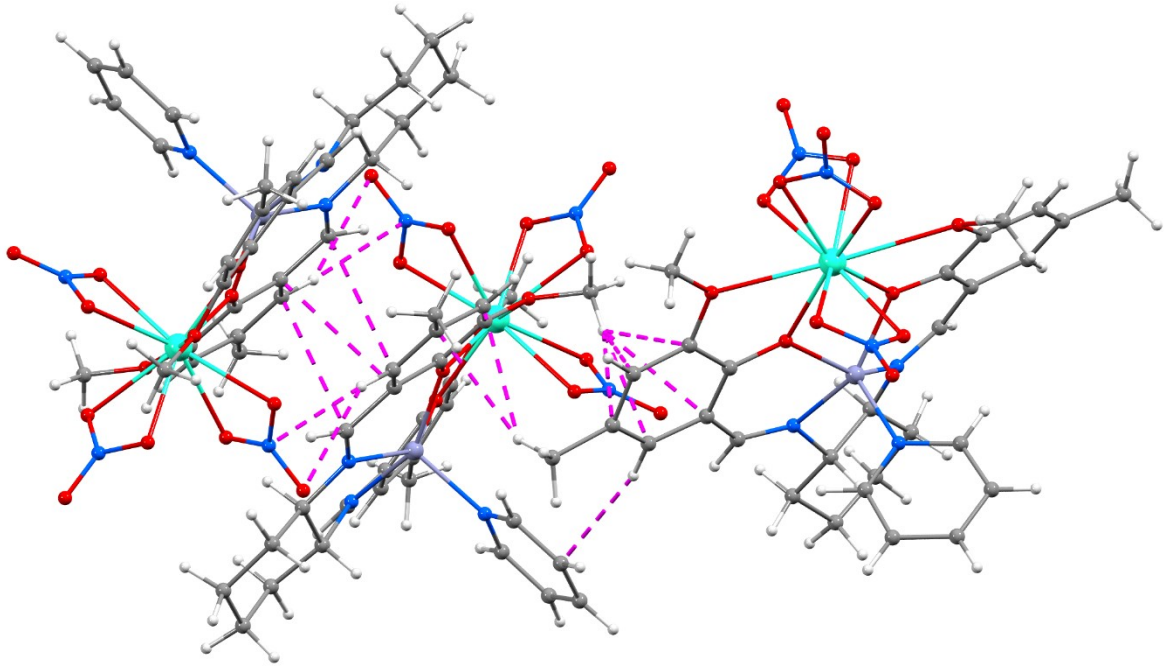

Fig. S8. A part of molecular packing showing different non-covalent interactions in 4.

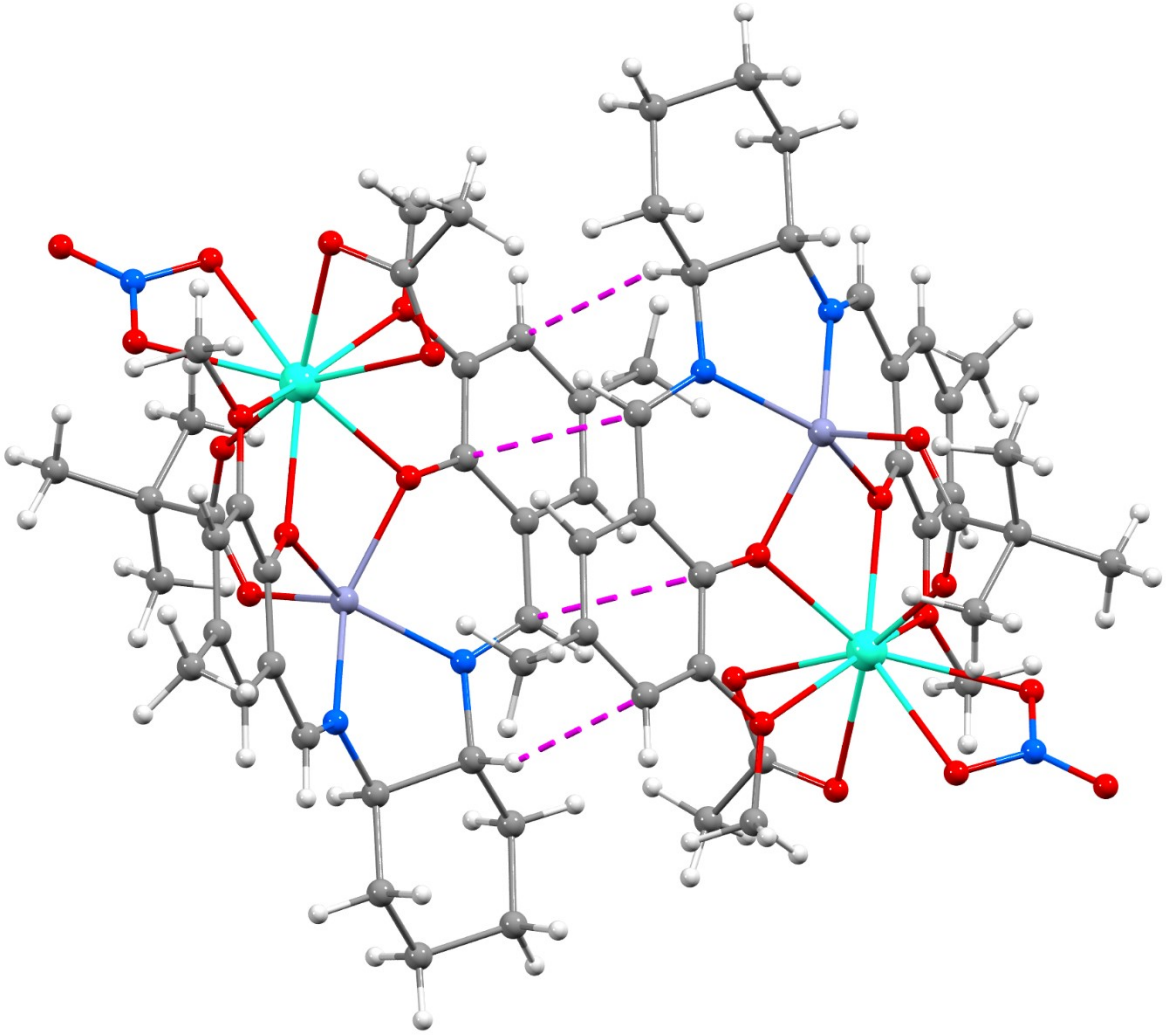

Fig. S9. A part of molecular packing showing different non-covalent interactions in **5**.

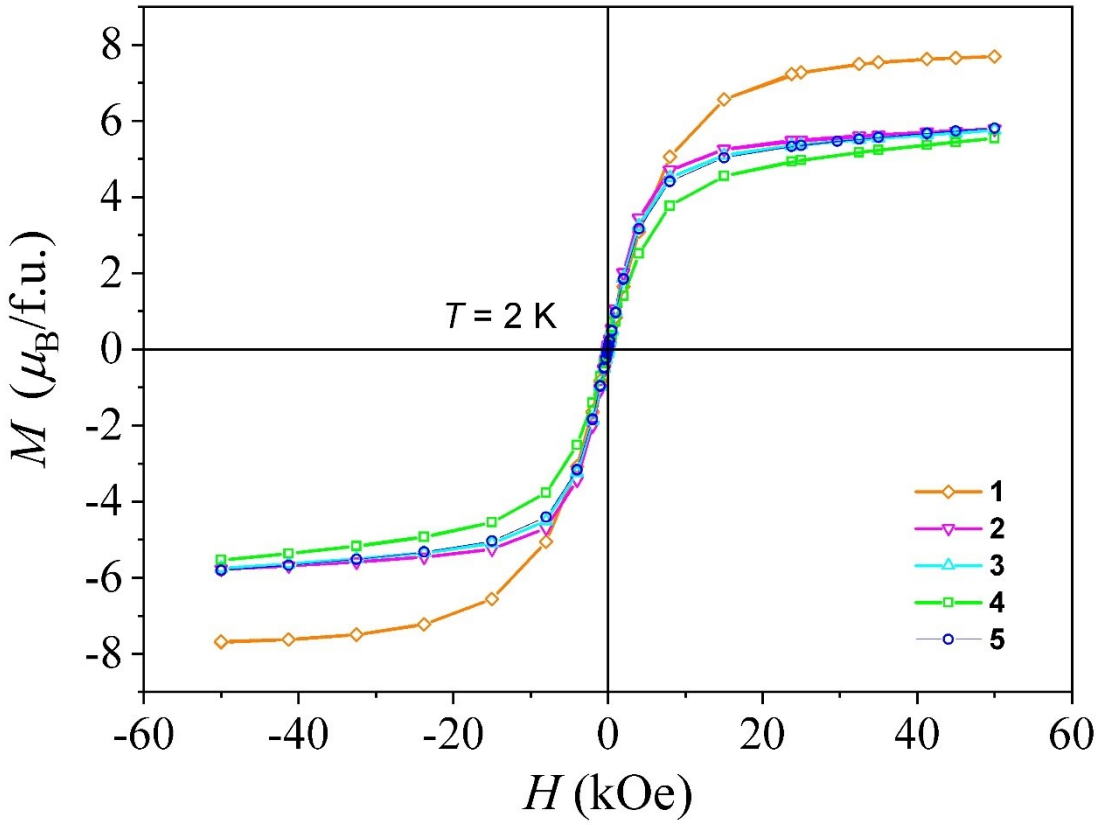

Fig. S10. Isothermal magnetization plots for **1-5** at 2 K.

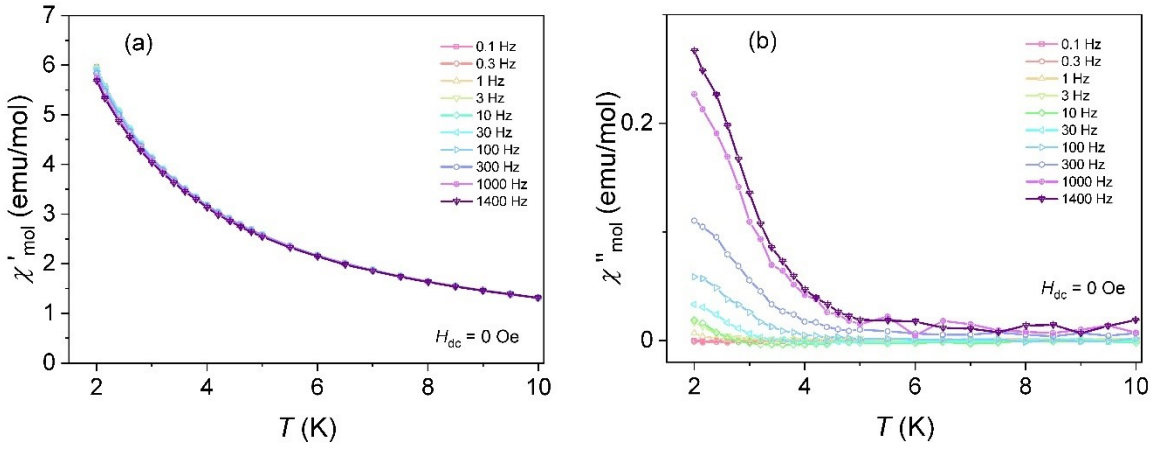

Fig. S11. Temperature dependence ac susceptibilities plots for complex 2 at zero dc field.

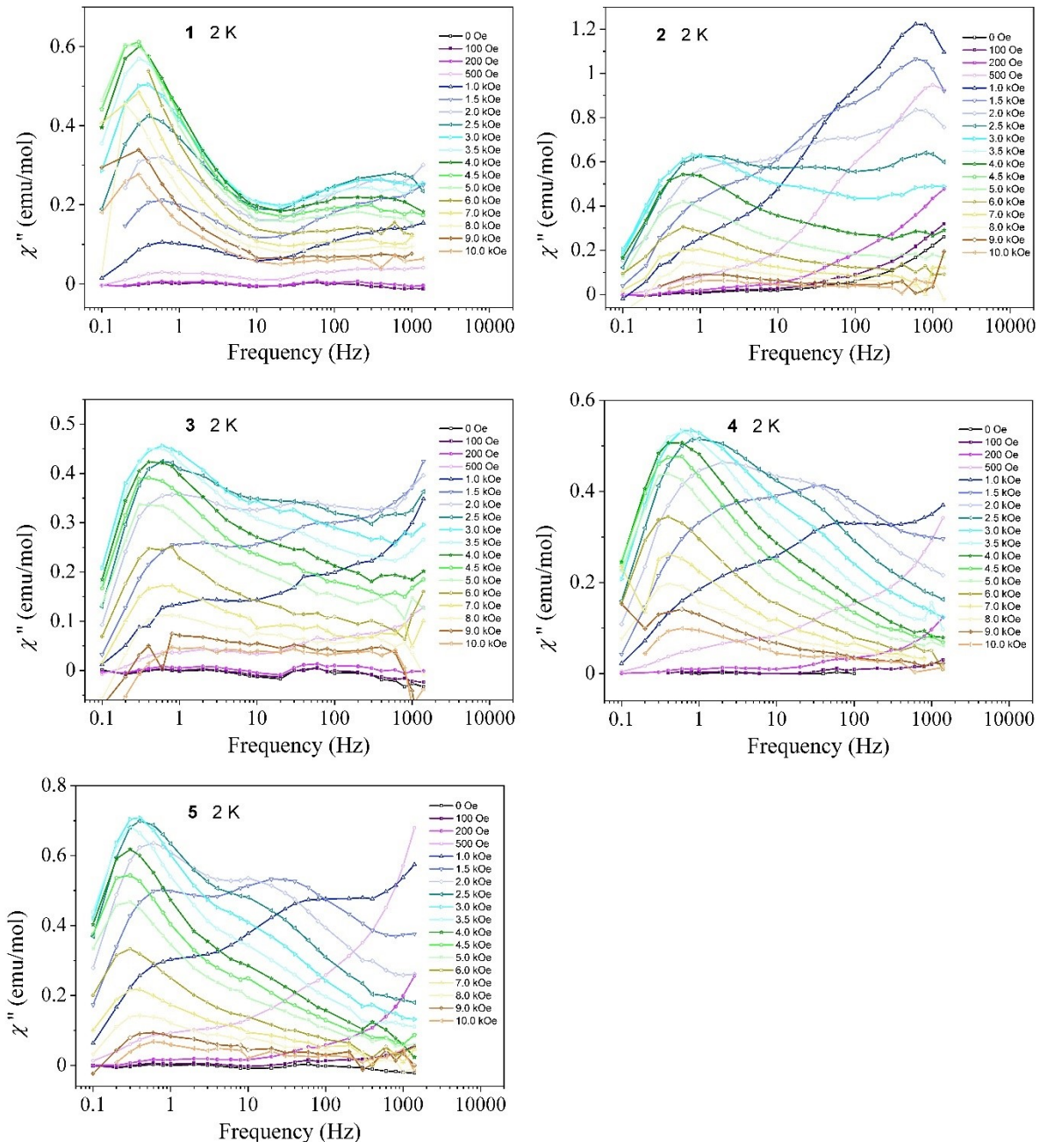

Fig. S12. Frequency dependent out-of-phase ac susceptibility plots of **1-5** at 2 K and at indicated magnetic fields.

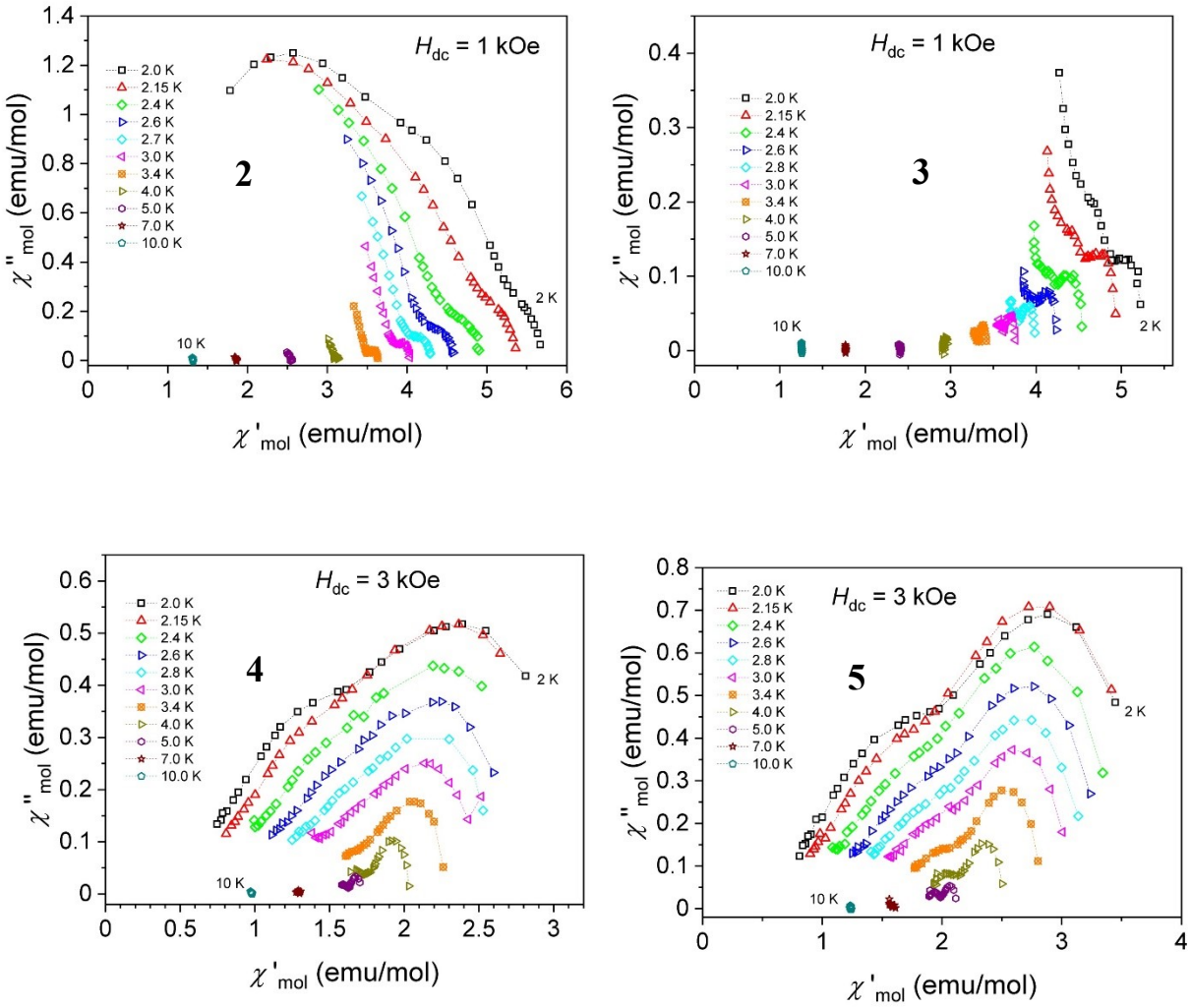

Fig. S13. The Cole-Cole plots for 2-5 at indicated magnetic fields.

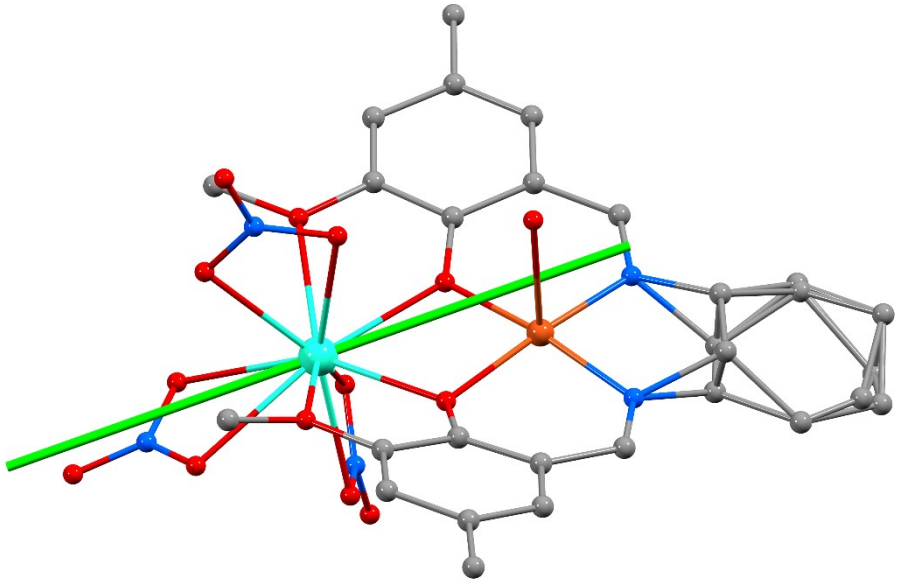

Fig. S14. The orientation of the principal magnetic axis of the ground Kramers doublet on the Dy^{III} center in complex **1** determined using MAGELLAN program.

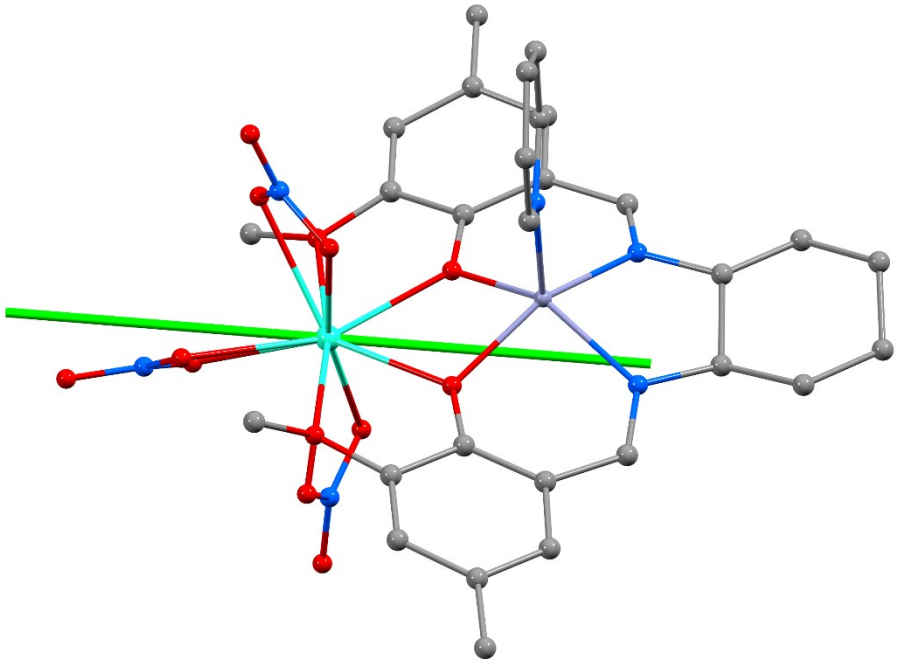

Fig. S15. The orientation of the principal magnetic axis of the ground Kramers doublet on the Dy^{III} center in complex **4** determined using MAGELLAN program.

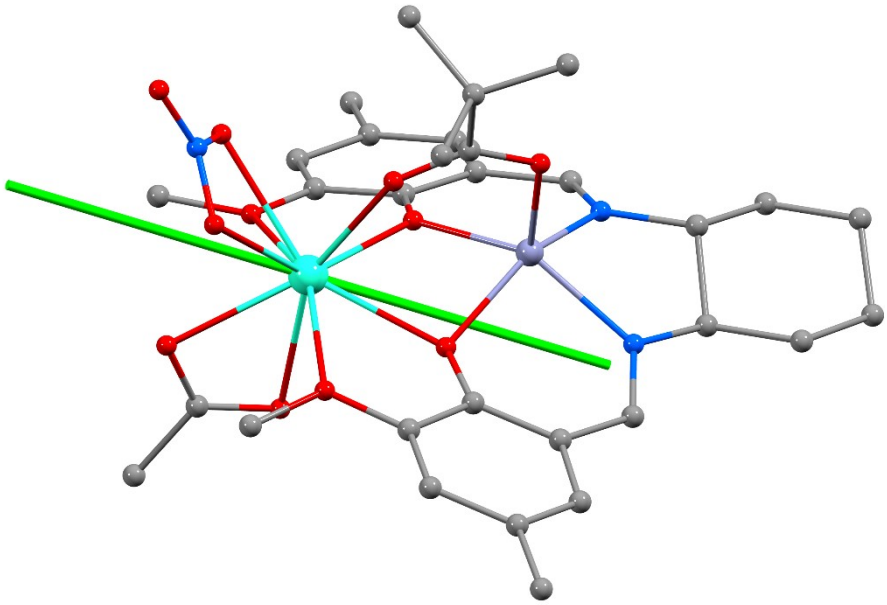

Fig. S16. The orientation of the principal magnetic axis of the ground Kramers doublet on the Dy^{III} center in complex **5** determined using MAGELLAN program.

Table S1. X-ray crystallographic data and refinement details for **1-5.**

	1	**2**	**3**	**4**	**5**
Empirical formula	$C_{24}H_{30}CuGdN_{14}$	$C_{24}H_{30}CuN_5O_{14}Tb$	$C_{24}H_{30}CuDyN_5O_4$	$C_{29}H_{33}DyN_6O_{13}Zn$	$C_{31}H_{40}DyN_3O_{11}Zn$
Formula weight	833.32	834.99	838.57	901.48	858.53
Temperature/K	150.00	150.00	150.00	150.00	150.00
Crystal system	monoclinic	monoclinic	monoclinic	monoclinic	Triclinic
Space group	$P2_1/n$	$P2_1/n$	$P2_1/n$	$P2_1/n$	$P\bar{1}$
a/Å	11.0211(14)	10.9930(9)	11.0363(9)	11.7307(9)	11.307(13)
b/Å	17.798(2)	17.7673(13)	17.7751(13)	18.1757(15)	12.824(15)
c/Å	15.593(2)	15.5779(12)	15.5230(11)	15.7891(13)	12.936(16)
α/°	90	90	90	90	91.62(3)
β/°	93.331(4)	92.795(3)	93.085(3)	94.240(3)	113.14(3)
γ/°	90	90	90	90	98.79(3)
Volume/Å^3	3053.5(7)	3039.0(4)	3040.8(4)	3357.2(5)	1696(3)
Z	4	4	4	4	2
ρ_{calc} g/cm^3	1.813	1.825	1.832	1.784	1.681
μ/mm^{-1}	2.925	3.084	3.213	2.997	2.954
F(000)	1656.0	1660.0	1664.0	1796.0	862
Crystal size	0.4 × 0.3 × 0.02	0.2 × 0.16 × 0.06	0.3 × 0.2 × 0.02	0.2 × 0.1 × 0.04	0.22 × 0.14 × 0.03
Radiation	MoKα (λ = 0.71073)	MoKα (λ = 0.71073)	MoKα (λ = 0.71073)	MoKα (λ = 0.71073)	MoKα (λ = 0.71073)
2Θ range /°	4.966 to 52.858	4.36 to 54.41	4.348 to 54.276	5.176 to 58.426	4.082 to 54.46
Reflections collected	43455	56456	65704	79540	87707
Independent reflections	6271 [R_{int}=0.0499, R_{sigma}=0.0344]	6702 [R_{int} = 0.0471, R_{sigma} = 0.0264]	6719 [R_{int} = 0.0457, R_{sigma} = 0.0255]	9018 [R_{int} = 0.0249, R_{sigma} = 0.0139]	7565 [R_{int} = 0.0318, R_{sigma} = 0.0149]
Data/restraints/parameter	6271/304/465	6702/315/465	6719/257/465	9018/324/516	7565/37/442
Goodness-of-fit on F^2	1.101	1.130	1.065	1.054	1.133
Final R indexes [I>=2σ (I)]	R_1 = 0.0402, wR_2 = 0.0871	R_1 = 0.0506, wR_2 = 0.1127	R_1 = 0.0315, wR_2 = 0.0745	R_1 = 0.0292, wR_2 = 0.0752	R_1 = 0.0290, wR_2 =0.0658
Final R indexes [all data]	R_1 = 0.0578, wR_2 = 0.0962	R_1 = 0.0643, wR_2 = 0.1204	R_1 = 0.0477, wR_2 = 0.0835	R_1 = 0.0316, wR_2 = 0.0770	R_1 = 0.0346, wR_2 =0.0704
Largest diff. peak/hole / e Å^{-3}	1.47/–1.28	1.18/–1.31	1.46/–1.21	2.20/–1.12	1.48/–0.83

Table S2. Bond distances around metal coordination spheres in **1−3.**

Bond	**1**	**2**	**3**
Ln–O1	2.566(3)	2.719(5)	2.724(3)
Ln–O2	2.333(3)	2.343(4)	2.337(3)
Ln–O3	2.364(3)	2.311(5)	2.305(3)
Ln–O4	2.716(3)	2.547(5)	2.553(3)
Ln–O5	2.510(5)	2.442(6)	2.429 (3)
Ln–O6	2.463(4)	2.523(6)	2.499(4)
Ln–O8	2.510(4)	2.536(5)	2.531(3)
Ln–O9	2.557(4)	2.491(6)	2.476(3)
Ln–O11	2.496(4)	2.450(6)	2.463(4)
Ln–O12	2.414(4)	2.407(6)	2.386(3)
Cu–O2	1.904(3)	1.919(5)	1.927(3)
Cu–O3	1.924(4)	1.893(5)	1.899(3)
Cu–O14	2.412(4)	2.387(6)	2.410(3)
Cu–N1	1.914(5)	1.917 (6)	1.920(4)
Cu–N2	1.928(5)	1.919(7)	1.913 (4)
Ln···Cu	3.412(4)	3.388(8)	3.386(5)

Table S3. Bond distances around metal coordination spheres in **4** and **5.**

Bond	**4**	**5**
Dy–O1	2.817(2)	2.542(3)
Dy–O2	2.3102(19)	2.312(3)
Dy–O3	2.311(2)	2.296(3)
Dy–O4	2.730(2)	2.625(4)
Dy–O5	2.441(2)	2.398(3)
Dy–O6	2.467(2)	2.357(3)
Dy–O8	2.464(2)	2.473(4)
Dy–O9	2.462(2)	2.464(3)
Dy–O11	2.424(3)	2.310(4)
Dy–O12	2.452(3)	-
Zn–O2	2.0033(19)	2.001(3)
Zn-O3	2.023(2)	2.032(3)
Zn-N1	2.045(3)	2.058(3)
Zn –N2	2.020(3)	2.016(3)
Zn –N3	2.049(3)	-
Zn-O10	-	1.995(3)
Dy···Zn	3.422(3)	3.341(3)

Table S4. Shape analysis around the Ln^{III} ions in **1-4**

Label	Shape	Symmetry	**1**	**2**	**3**	**4**
DP-10	Decagon	D_{10h}	32.790	32.966	32.949	35.211
EPY-10	Enneagonalpyramid	C_{9V}	23.822	23.882	24.014	25.624
OBPY10	Octagonalbipyramid	D_{8h}	16.919	16.971	17.026	17.092
PPR-10	Pentagonal prism	D_{5h}	8.411	8.517	8.399	10.296
PAPR-10	Pentagonalantiprism	D_{5d}	13.343	13.480	13.339	8.355
JBCCU-10	Bicappedcube J15	D_{4h}	12.432	12.728	12.942	5.895
JBCSAPR-10	Bicapped square antiprism	D_{4d}	6.414	6.490	6.460	3.729
JMBIC-10	Metabidiminished icosahedron	C_{2V}	8.552	8.782	8.873	5.235
JATDI-10	Augmented tridiminished icosahedron	C_{3V}	16.822	17.049	17.115	19.025
JSPC-10	Sphenocorona J87	C_{2V}	**2.858**	**2.707**	**2.765**	4.380
SDD-10	Staggered Dodecahedron	D_2	5.143	5.302	5.249	**3.570**
TD-10	Tetradecahedron	C_{2V}	4.483	4.620	4.588	**3.530**
HD-10	Hexadecahedron	D_{4h}	9.359	9.639	9.748	4.247

Table S5. Shape analysis around the Dy^{III} ion in **5.**

Label	Shape	Symmetry	**5**
EP-9	Enneagon	D_{9h}	34.096
OP-9	Octagonal pyramid	C_{8V}	24.465
HBPY-9	Heptagonal bipyramid	D_{7h}	15.661
JTC-9	Johnson triangular cupola	C_{3V}	14.540
JCCU-9	Capped cube	C_{4V}	7.908
CCU-9	Spherical-relaxed capped cube	C_{4V}	6.582
JCSAPR-9	Capped square antiprism	C_{4V}	4.123
CSAPR-9	Spherical capped square antiprism	C_{4V}	**3.251**
JTCTPR-9	Tricapped trigonal prism	D_{3h}	3.980
TCTPR-9	Spherical tricapped trigonal prism	D_{3h}	**3.021**
JTDIC-9	Tridiminshed icosahedron	C_{3V}	10.997
HH-9	Hula-hoop	C_{2V}	7.209
MFF-9	Muffin	C_S	**3.241**

Table S6. Relaxation fitting parameters from the least-square fitting of the Cole-Cole plots of **1** by the double-component generalized Debye model at 5 kOe dc field.

T (K)	χ_S (emu/mol)	$\Delta\chi$ (emu/mol)	τ (s)	α	$\Delta\chi$ (emu/mol)	τ (s)	α
2	0.53053	1.21551	6.59E-04	0.58421	1.57112	0.86605	0.17072
2.15	0.26573	1.53738	4.14E-04	0.71321	1.45078	0.69405	0.11698
2.4	0	1.98438	2.08E-04	0.78045	1.27618	0.53912	0.0772
2.6	0	1.80199	7.23E-05	0.73944	1.20733	0.48193	0.14408
2.8	0	1.79317	4.64E-05	0.73123	1.07479	0.40753	0.14426
3	0	1.74837	2.86E-05	0.70523	0.98573	0.36835	0.16559
3.2	0	1.69142	1.75E-05	0.68218	0.91783	0.32398	0.17091
3.4	0	1.6208	1.18E-05	0.63681	0.87103	0.28751	0.19664
3.6	0	1.7814	7.79E-06	0.74022	0.58581	0.27258	0
3.8	0	1.82058	2.54E-06	0.78949	0.49549	0.26787	0
4	0	1.56137	6.88E-06	0.50326	0.65905	0.26309	0.21442
4.2	0	1.57114	9.59E-06	0.44089	0.55982	0.26433	0.22928
4.4	0	1.57848	9.02E-06	0.41594	0.44024	0.24229	0.19831
4.6	0	1.57208	1.05E-05	0.36642	0.3796	0.25324	0.22117
4.8	0	1.56403	1.03E-05	0.34811	0.31429	0.261	0.21633
5	0	1.53574	1.52E-05	0.21937	0.30272	0.309	0.3038
5.5	0	1.48901	8.40E-06	0.26939	0.17477	0.30019	0.24564
6	0	1.41792	9.00E-06	0.15672	0.1223	0.35936	0.29309
6.5	0	1.34817	8.55E-06	0.16915	0.07879	0.37395	0.25884

Table S7. Magneto-structural data on heterobimetallic M-Gd^{III} (M = 3d ion) systems displaying slow relaxation of magnetization (SRM) with non-Orbach relaxation mechanism.

Complex	Geometry of M^{n+}/Gd^{3+} ions	M-Gd interaction	SRM via power law mechanism ($\tau^{-1} \propto T^n$)	Additional relaxation path	Applied Field (Oe)	ref
$[Ni(o\text{-}van\text{-}en)GdCl_3(H_2O)]$	SP-4/BTPR-8	-	n = 10.8(3)	QTM	1500	S1
$\{[Gd(H_2O)_3\{Cu(pyzha)\}5(MeOH)_3]\cdot 3(TfO)\cdot 3(H_2O)\}_n$	5-coordinate/8-coordinate	F	-	-	1000	S2
$[CuL^1(\mu\text{-}NO_3)Ln(NO_3)_2(H_2O)]\cdot CH_3CN$	SPY-5/ JSPC-10	F	n = 4	-	5000	S3
$[CuL^2(\mu\text{-}NO_3)Ln(NO_3)_2(H_2O)]\cdot CH_3CN$	SPY-5/ JSPC-10	F	n = 4	-	5000	S3
$[NaGd(VO)_2(cbdc)_4(H_2O)_{10}]_n$	Oh-6/TDD-8	F	n = 1	Orbach	5000	S4
$\{[RbGd(VO)_2(cbdc)4(H_2O)_{10}]2.5H_2O\}_n$	Oh-6/ BTPR-8	F	n = 2.32	Orbach	2500	S4
$\{[CsGd(VO)_2(cbdc)4(H_2O)_{11}]5H_2O\}_2$	Oh-6/ SAPR-8	AF	n = 1	Orbach	2500	S4
$[Cu(L^3)Gd(NO_3)_3]_2$	SYP-5/SDD-10	F	-	-	6000	S5
$[Gd_2Ni_3(dto)_6(H_2O)_{10}]\cdot 12H_2O$	SP-4/CSAPR-9 or MFF-9	-	2.38	-	2500	S6
$[Gd_2Ni_3(dto)_6(H_2O)_{10}]\cdot 2H_2O$			1.87	-	2500	S6
$[Fe^{III}_4Ln^{III}_4(teaH)_8(N_3)_8(H_2O)]$	Oh-6/ SAPR-8 and CSAPR-9	F	-	-	-	S7
$[Gd(ZnL^4)_2]CF_3SO_3\cdot 0.5H_2O$	-	-	1.56	-	1000	S8
$[CuGd(H_2L^5)(NO_3)_3]\cdot 2MeOH$	SP-4/ TD-10	F	8.8	-	1000	S9
$[NiGd(H_2L^5)(NO_3)_3]\cdot 4MeOH$	SP-4/ TD-10	weak	9.0	-	5000	S9
$[CuLn(L^6)(NO_3)_3(H_2O)]$	SPY-5/JSPC-10	F	-	-	5000	S10
$[Cu_6M_4(pypt)_4(pypdH)_4(NO_3)_8]$	SPY-5/TDD-8	F	-	-	2000	S11

[H_2(o-van-en) = N,N'-ethylene-bis(3-methoxysalicylaldiminate); (H2pyzha) = pyrazinohydroxamic acid; L^1 = N-salicylidene-N′-3-methoxysalicylidenepropane-1,2-diamine; L^2 = N-3-methoxysalicylidene-N′-salicylidenepropane-1,2-diamine; cbdc = cyclobutane-1,1-dicarboxylic acid salts; H_2L^3 = 2-(((4-(4-((2-(oxido)-3-methoxybenzylidene)amino)phenoxy)phenyl)-imino)methyl)-6-methoxyphenolato; dto = dithiooxalate; $teaH_3$ = triethanolamine; H_3L^4 = tris(((2-hydroxy-3-methoxybenzyl)-amino)ethyl)amine; H_4L^5 = (3,3′-((1*E*,1′*E*)-(ethane-1,2-diylbis-(azaneylylidene)) bis(methaneylylidene))bis(benzene-1,2-diol)); H_2L^6 = *N,N*′-bis(3-methoxy-5-methylsalicylidene)-1,2-phenylenediamine; $pypdH_2$ = 2-(2-pyridyl)-1,3-propane-diol; $pyptH_3$ = 2-hydroxymethyl-2-(2-pyridyl)-1,3-propane-diol.

TableS8: List of important geometrical features and relevant magnetic parameters of heterobimetallic $Cu^{II}Ln^{III}$ complexes displaying slow relaxation of Magnetization (SRM).

Complex	Geometry of Cu^{II}/Ln^{II} ions	Cu-Ln interaction	U_{eff} /K	Applied Field Oe)	ref
$[CuLn(hmp)_2(NO_3)_3(H_2O)_2]$	SP-4 /JSPC-10	F	No Max.	-	S12
$[L^7Cu(O_2COMe)Tb(thd)_2]$	SPY-5/MFF-9	F	13.8	1000	S13
$[TbCu(L^8)_2(NO_3)_3$	Oh-6/CSAPR-10	F	16.6(5)	1000	S14
$[TbCu(L^9)(NO_3)_3(H_2O)$	SPY-5/JSPC-10	F	29(2),	1000	S15
$[TbCu(L^9)(NO_3)$(o-vanilate)(MeOH)]NO_3	SPY-5/CSAPR-9	F	32.2(6)	1000	S15
$[TbCu(sal)(NO_3)_2(L^9)(MeOH)]$	SPY-5/CSAPR-9	F	32.9(4)	1000	S16
$[DyCu(sal)(NO_3)_2(L^9)(MeOH)]$	SPY-5/CSAPR-9	F	26.0(5)	1000	S16
$[Cu(L^{10})(C_3H_6O)Tb(NO_3)_3]$	SPY-5/TD-10	F	42.3(4),	1000	S17
$[Cu(L^{10})(C_3H_6O)Dy(NO_3)_3]$	SPY-5/TD-10	F	11.5(10),	1000	S17
$[DyCuL^{11}(OAc)_2(NO_3)]$	SPY-5/CSAPR-9	F	No Max.	1750	S18
[Cu(3-MeOsaltn)(ac)$Tb(hfac)_2$].	SPY-5/CSAPR-9	F	No Max.	1000	S19
[Cu(3-MeOsaltn)(ac)$Dy(hfac)_2$].	SPY-5/CSAPR-9	F	No Max.	1000	S19
$[CuDy(HL^{12})(H_2O)(NO_3)_3]$	SPY-5/JSPC-10	F	122(1)	2000	S20
$[(CuL^{13})Tb(NO_3)_3]$	SP-4/TCTPR-9	F	28.5(5),	2000	S21
$[(CuL^{13})Dy(NO_3)_3]$	SP-4/TCTPR-9	F	53(2),	2000	S21
$[CuL^{14}(\mu\text{-}NO_3)Tb(NO_3)_2(H_2O)]\cdot CH_3CN$	SPY-5/JSPC-10	F	19.3(8)	2000	S22
$[CuL^{14}$ $(\mu\text{-}NO_3)Dy(NO_3)_2(H_2O)]\cdot CH_3CN$	SPY-5/JSPC-10	F	26.1(10)	2000	S22
$[CuL^{15}(\mu\text{-}NO_3)Tb(NO_3)_2(H_2O)]\cdot CH_3CN$	SPY-5/JSPC-10	F	23.8(10),	2000	S22
$[CuL^{15}(\mu\text{-}NO_3)Dy(NO_3)_2(H_2O)]\cdot CH_3CN$	SPY-5/JSPC-10	F	28.2(5),	2000	S22
[Cu(Cl)(valen)$Tb(NO_3)(CH_3OH)(H_2O)$(dca)]	SP-4/ JSPC-10	F	21.85	0	S23
$[Ln(hfac)_3Cu(acac)_2]$	SPY-5/ TDD-8	AF	105(26)	2000	S24
$[CuTb(L^6)(NO_3)_3(H_2O)]$	SPY-5/JSPC-10	F	5.3#	1000	S10
$[CuDy(L^6)(NO_3)_3(H_2O)]$	SPY-5/JSPC-10	F	6.7#	3000	S10
$[CuTb(H_2L^{16})(NO_3)_3]\cdot 2MeOH$	SP-4/TD-10	F	non-Orbach	1500	S25

Estimated using modified Arrhenius law: $\ln(\chi''/\chi') = \ln(\omega\tau_0) + U_{eff}/kT$

Hmp = 2-(hydroxymethyl)-pyridine; $(L^7)^{2-}$ = N,N′-2,2-dimethylpropylenedi(3-methoxysalicylideneiminato); L^8 = 2-methoxy-6-(((3-methoxypropyl)imino)methyl)phenol; L^9 = ((2,2-dimethylpropane-1,3-diyl)bis(azaneylylidene))bis(methaneylylidene))bis(2-methoxyphenol); sal = salicylate; H_2L^{10} = N,N′-bis(3-methoxysalicylidene)-1,3-diamino-2,2-dimethylpropane; H_2L^{11} = N,N-bis(3-methoxysalicylidene)-1,2-cyclohexanediamine; 3-MeOsaltn = N,N′-bis(3-methoxy-2-oxybenzylidene)-1,3-propanediaminato; ac = acetate; hfac = hexafluoroacetylacetonato; H_3L^{12} = ((2-hydroxypropane-1,3-diyl)bis(azaneylylidene))bis(methaneylylidene))bis(2-methoxyphenol); H_2L^{13} = N-α-methylsalicylidene-N0-3-methoxysalicylidene-1,3-propanediamine; H_2L^{14} = *N*-salicylidene-*N′*-3-ethoxysalicylidene-1,3-propanediamine; H_2L^{15} = *N*-salicylidene-*N′*-3-methoxysalicylidene-1,3-propanediamine; H_2valen = 1,2-ethanediylbis(2-iminomethylene-6-methoxy-phenol); dca = dicyanamide; acac = acetylacetonato; H_4L^{15} = (3,3′-((1*E*,1′*E*)-(ethane-1,2-diylbis-(azaneylylidene)) bis(methaneylylidene))bis(benzene-1,2-diol)).

References:

S1. A. Vráblová, M. Tomás, L. R. Falvello, L. Dlháň, J. Titiš, J. Černák and R. Boča, *Dalton Trans.*, 2019, **48**, 13943.

S2 H.-G. Zhang, H. Yang, L. Sun, D.-C. Li and J.-M. Dou, *Eur. J. Inorg. Chem.*, 2019, **23**, 2839–2843.

S3 T. K. Ghosh, S. Maity, J. Mayans and A. Ghosh, *Inorg. Chem.*, 2021, **60**, 438–448.

S4 E. S. Bazhina, A. A. Korlyukov, J. K. Voronina, K. A. Babeshkin, E. A. Ugolkova, N. N. Efimov, M. V. Fedin, M. A. Kiskin and I. L. Eremenko, *Magnetochemistry*, 2021, **7**, 82.

S5 S. Caballero, E. Pilichos, M. Font-Bardia, J. Mayans and A. Escuer, *Cryst. Growth Des.*, 2023, **23**, 3711–3719.

S6 N. El A.-Dahmouni, R. Rabelo, J. Mayans, N. Moliner, S.-E. Stiriba, M. Julve, A. Switlicka, B. Machura, R. R.-Garcia, and Joan Cano, *Cryst. Growth Des.* 2023, **23**, 5403−5408.

S7 D. Schray, D. Westerbeck, J. Braun, Y. Lan, S. Gómez-Coca, W. Wernsdorfer, E. Ruiz, C. E. Anson, J. Schnack and A. K. Powell, *Inorg. Chem.*, 2023, **62**, 6642–6648.

S8 Y. Masuda, S. Sakata, S. Kayahara, N. Irie, M. Kofu, Y. Kono, T. Sakakibara, Y. Horii and T. Kajiwara, *J. Phys. Chem. C*, 2023, **127**, 3295–3306.

S9 E. C.-Villén, M F.-Bardia, J. Mayans and A. Escuer, *Cryst. Growth Des.* 2024, **24**, 5806−5817.

S10 N. C. Jana, Z. Jagličić, R. Herchel, P. Brandão, R. Nandy and A. Panja, *Cryst. Growth Des.*, 2024, **24**, 7537–7548.

S11 A. Anastassiades, D. I. Alexandropoulos, C. D. Buch, S. Piligkos, A. J. Tasiopoulos, *Dalton Trans*., 2024, **53**, 16202–16211.

S12 F. He, M.-L. Tong and X.-M. Chen, *Inorg. Chem.*, 2005, **44**, 8285–8292.

S13 J.-P. Costes, F. Dahan and W. Wernsdorfer, *Inorg. Chem.*, 2006, **45**, 5–7.

S14 T. Kajiwara, M. Nakano, S. Takaishi and M. Yamashita, *Inorg. Chem.*, 2008, **47**, 8604–8606.

S15 T. Kajiwara, K. Takahashi, T. Hiraizumi, S. Takaishi and M. Yamashita, *Polyhedron*, 2009, **28**, 1860–1863.

S16 T. Kajiwara, M. Nakano, K. Takahashi, S. Takaishi and M. Yamashita, *Chem. Eur. J.*, 2011, **17**, 196–205.

S17 T. Ishida, R. Watanabe, K. Fujiwara, A. Okazawa, N. Kojima, G. Tanaka, S. Yoshi and H. Nojiri, *Dalton Trans.*, 2012, **41**, 13609–13619.

S18 P. Zhang, L. Zhang, S.-Y. Lin and J. Tang, *Inorg. Chem.*, 2013, **52**, 6595–6602.

S19 M. Towatari, K. Nishi, T. Fujinami, N. Matsumoto, Y. Sunatsuki, M. Kojima, N. Mochida, T. Ishida, N. Re and J. Mrozinski, *Inorg. Chem.*, 2013, **52**, 6160–6178.

S20 M. Dolai, M. Ali, J. Titiš and R. Boča, *Dalton Trans.*, 2015, **44**, 13242–13249.

S21 P. Mahapatra, N. Koizumi, T. Kanetomo, T. Ishida and A. Ghosh, *New J. Chem.*, 2019, **43**, 634–643.

S22 S. Maity, P. Bhunia, K. Ichihashi, T. Ishida and A. Ghosh, *New J. Chem.*, 2020, **44**, 6197–6205.

S23 S.-L. Zhang, X.-F. Fan, R.-L. Du, B.-W. Shen, X.-D. Song, X.-Q. Wei and S.-S. Li, *Polyhedron*, 2021, **206**, 115336.

S24 L. Bellucci, L. Giordano, S. Carlotto, G. Poneti, M. Rancan, S. Samaritani, L. Armelao and L. Labella, *Inorg. Chim. Acta*, 2023, **556**, 121665.

S25 E. Costa-Villén, M. Font-Bardia, J. Mayans and A. Escuer, *Cryst. Growth Des.*, 2024, **24**, 5806–5817.